# Two New Three-Dimensional Vanadium(III) and Iron(III) Phosphites Templated by Ethylenediamine: $(C_2H_{10}N_2)_{0.5}[M(HPO_3)_2]$. Ab Initio Structure Determination, Spectroscopic, and Magnetic Properties

Sergio Fernández,[†] José L. Mesa,[†] José L. Pizarro,[‡] Luis Lezama,[†] María I. Arriortua,[‡] and Teófilo Rojo*,[†]

*Departamentos de Química Inorgánica and Mineralogía-Petrología, Facultad de Ciencias, Universidad del País Vasco, Apdo. 644, E-48080 Bilbao, Spain*

*Received November 22, 2001. Revised Manuscript Received February 1, 2002*

The $(C_2H_{10}N_2)_{0.5}[M(HPO_3)_2]$ (M = V, Fe) inorganic−organic hybrid compounds have been synthesized under mild hydrothermal conditions. The crystal structure determination of the vanadium phase has been carried out from X-ray powder diffraction data by using the ab initio method. A Rietveld full-profile refinement has been performed on the isostructural iron compound. The unit-cell parameters are $a = 9.243(1)$, $b = 8.817(1)$, $c = 9.684(1)$ Å, and $\beta = 120.92(2)°$ and $a = 9.247(1)$, $b = 8.824(1)$, $c = 9.693(1)$ Å, and $\beta = 120.72(1)°$ for the vanadium and iron compounds, respectively. Both compounds are monoclinic, $P2/c$ with $Z = 4$. The crystal structure consists of a three-dimensional framework with channels along the $c$ axis where the ethylenediammonium cations are located. The metallic ions are interconnected by the pseudopyramidal $(HPO_3)^{2-}$ phosphite anions and adopt a tetrahedral-like−diamond distribution. The IR and Raman spectra of both phases show the bands corresponding to the phosphite oxoanions and ethylenediammonium cations. The diffuse reflectance spectra in the visible region are consistent with the existence of vanadium(III) and high-spin iron(III) cations in slightly distorted octahedral coordination. Magnetic measurements indicate the existence of antiferromagnetic interactions being stronger in the iron compound.

## Introduction

Open-framework materials are of great interest from both the industrial and academic point of view due to their catalytic, adsorbent, and ion-exchange properties. While the large voids, chemical stability, and size discriminatory absorptive behavior of zeolites render them very useful, open-framework solids containing transition elements could provide novel properties including catalytic, electronic, and magnetic properties inaccessible in main group systems. This has directed recent efforts at the preparation of non-silicate materials with the goal of preparing solids with larger dimensionalities on unique framework topologies or novel polyhedral connectivities.[1]

Since the discovery of the microporous aluminophosphates by Wilson et al.,[2] great interest has been aroused in the synthesis of new transition-metal phosphates templated by organic amines. Much less exploratory work has been carried out on the oxo-anion part of the inorganic network and the phosphate anion is ubiquitous in these materials.[3] The possibilities of incorporating the phosphorus(III)-containing pseudopyramidal $(HPO_3)^{2-}$ hydrogen phosphite group into extended structures were demonstrated several years ago.[4] In these materials the organic amine resides within the inorganic skeleton, playing a structure-directing, space-filling, and charge-balancing role.

The inorganic−organic hybrid phosphites with metallic transition elements have not been extensively studied, and only compounds with the V(IV), Co(II), and Mn(II) cations are known.[5] To complete the knowledge about this type of microporous materials incorporating metallic magnetic cations belonging to the first series

* To whom correspondence should be addressed.
[†] Departamento de Química Inorgánica.
[‡] Departamento de Mineralogía-Petrología.

(1) (a) Cheetham, A. K.; Ferey, G.; Loiseau, T. *Angew. Chem., Int. Ed.* **1999**, *38*, 3268. (b) Davis, M. E.; Lobo, R. F. *Chem. Mater.* **1992**, *4*, 756. (c) Venuto, P. B. *Microporous Mater.* **1994**, *2*, 297. (d) Smith, J. V. *Chem. Rev.* **1988**, *88*, 149.

(2) (a) Wilson, S. T.; Lok, B. M.; Messian, C. A.; Cannan, T. R.; Flanigen, E. M. *J. Am. Chem. Soc.* **1982**, *104*, 1146. (b) Wilson, S. T.; Lok, B. M.; Flanigen, E. M. U.S. Patent 4310440, 1982.

(3) (a) Bonavia, G.; Haushalter, R. C.; O'Connor, C. J.; Zubieta, J. *Inorg. Chem.* **1996**, *35*, 5603. (b) Loiseau, T.; Ferey, G. *J. Solid State Chem.* **1994**, *111*, 416. (c) Natarajan, S.; Eswaramoorthy, M.; Cheetham, A. K.; Rao, C. N. R. *Chem. Commun.* **1998**, 1561. (d) Lii, K. H.; Huang, Y. F.; Zima, V.; Huang, C. Y.; Lin, H. M.; Jiang, Y. C.; Liao, F. L.; Wang, S. L. *Chem. Mater.* **1998**, *10*, 2599. (e) Leech, M. A.; Cowley, A. R.; Prout, C. K.; Chippindale, A. M. *Chem. Mater.* **1998**, *10*, 451. (f) Francis, R. J.; Drewitt, M. J.; Halasyamani, P. S.; Ranganathachar, C.; O'Hare, D.; Clegg, W.; Teat, S. J. *Chem. Commun.* **1998**, 279. (g) Lu, J. J.; Goh, N. K.; Chia, L. S. *Chem. Commun.* **1998**, 1709. For further examples, see ref 1a.

(4) (a) Shieh, M.; Martin, K. J.; Squattrito, P. J.; Clearfield, A. *Inorg. Chem.* **1990**, *29*, 958. (b) Sapiña, F.; Gomez, P.; Marcos, M. D.; Amoros, P.; Ibañez, R.; Beltran, D. *Eur. J. Solid State Inorg. Chem.* **1989**, *26*, 603. (c) Marcos, M. D.; Amoros, P.; Beltran, A.; Martinez, R.; Attfield, J. P. *Chem. Mater.* **1993**, *5*, 121. (d) Attfield, M. P.; Morris, R. E.; Cheetham, A. K. *Acta Crystallogr.* **1994**, *C50*, 981. (e) Marcos, M. D.; Amoros, P.; Le Bail, A. *J. Solid State Chem.* **1993**, *107*, 250.

10.1021/cm0112845 CCC: $22.00 
Published on Web 04/05/2002

of transition elements, we have synthesized the $(C_2H_{10}N_2)_{0.5}[M(HPO_3)_2]$ phosphites, where M is $V^{3+}$ and $Fe^{3+}$. The crystal structure determination of these compounds was carried out from powdered diffraction data by using an ab initio method. It is worth mentioning the existence of two sublattices with both tetrahedral and square-planar geometries. The spectroscopic and magnetic properties of both compounds are also discussed.

## Experimental Section

**Synthesis and Characterization.** The $(C_2H_{10}N_2)_{0.5}[M(HPO_3)_2]$ (M = V, Fe) compounds were prepared under mild hydrothermal conditions. The starting reagents were $VCl_3$ or $FeCl_3 \cdot 6H_2O$, $H_3PO_3$, and ethylenediamine in a molar ratio of 0.08:15.2:13.3 or 0.77:3.79:3.3 for the vanadium and iron phases, respectively. These reaction mixtures with a volumne of 30 mL of water for the vanadium compound or water:butanol (1:2) for the iron compound were stirred up to homogeneity. After that, they were placed in a PTFE-lined stainless steel pressure vessel (fill factor 75%) and heated at 170 °C for 5 days, followed by slow cooling to room temperature. The pH of the mixtures did not show any appreciable change during the hydrothermal reactions and remained at ≈6.0. Both compounds were obtained as homogeneous powdered samples with green and lightly green colors for the vanadium(III) and iron(III) phases, respectively. The percentage of the elements in the products were calculated by inductively coupled plasma atomic emission spectroscopy (ICP-AES) and C, H, N-elemental analysis. Found: V, 20.9; P, 25.3; C, 4.9; H, 2.7; N, 5.7. $(C_2H_{10}N_2)_{0.5}[V(HPO_3)_2]$ requires the following: V, 21.1; P, 25.6; C, 5.0; H, 2.9; N, 5.8. Found: Fe, 22.3; P, 24.9; C, 4.7; H, 2.6; N, 5.6. $(C_2H_{10}N_2)_{0.5}[Fe(HPO_3)_2]$ requires the following: Fe, 22.6; P, 25.1; C, 4.9; H, 2.8; N, 5.7. The densities were measured by flotation in mixtures of $CHCl_3/CHBr_3$ by using powdered samples as pellets obtained at 15 Kbar. The values are 2.28(2) and 2.26(3) $g \cdot cm^{-3}$ for the vanadium and iron compounds, respectively.

Thermogravimetric analysis of the compounds was carried out under an oxygen atmosphere in a SDC 2960 Simultaneous DSC-TGA TA Instrument. Crucibles containing ≈20 mg of sample were heated at 5 °C·min$^{-1}$ in the temperature range 30−800 °C. The decomposition of $(C_2H_{10}N_2)_{0.5}[V(HPO_3)_2]$ takes place in two superimposed steps with different speeds between 300 and 800 °C. The mass loss is 12.0%, in good agreement with the calcination of the ethylenediammonium cation (12.8%). The X-ray powder diffraction pattern of the residue obtained from the thermogravimetric analysis at 800 °C shows the existence of peaks belonging to $VO(PO_3)_2$ [$I\bar{4}2d$ space group with $a = b = 10.990(1)$ and $c = 4.258(1)$ Å] and $VOPO_4$ [*Pnma* space group with $a = 7.770(1)$, $b = 6.143(1)$, $c = 6.965(1)$ Å].[6a] The decomposition curve of $(C_2H_{10}N_2)_{0.5}[Fe(HPO_3)_2]$ reveals a mass loss of 12.5% between 300 and 670 °C, which agrees well with that calculated for the loss of the ethylenediammonium cation (12.6%). Between 670 and 800 °C, additional weight losses were not observed. The X-ray powder diffractogram of the residue obtained at 800 °C indicates the presence of $Fe(PO_3)_3$ and $Fe_2Fe(P_2O_7)_2$ [*Pnma* space group with $a = 8.950(1)$, $b = 12.235(1)$, and $c = 10.174(1)$ Å].[6b]

The thermal behavior of the $(C_2H_{10}N_2)_{0.5}[M(HPO_3)_2]$ (M = V and Fe) compounds has also been studied by using time-resolved X-ray thermodiffractometry in an air atmosphere. A PHILIPS X′PERT automatic diffractometer (Cu Kα radiation) equipped with a variable-temperature stage (Paar Physica TCU2000) with a Pt sample holder was used in the experiment. The powder patterns were recorded in 2$\theta$ steps of 0.02° in the range 5° ≤ 2$\theta$ ≤ 45°, counting for 1 s per step and increasing the temperature at 5 °C·min$^{-1}$ from room temperature up to 800 °C. The $(C_2H_{10}N_2)_{0.5}[V(HPO_3)_2]$ and $(C_2H_{10}N_2)_{0.5}[Fe(HPO_3)_2]$ compounds are stable up to 255 and 240 °C, respectively, and the intensity of the monitored (121) peak at 2$\theta$ = 27.8° for both vanadium and iron phases remains practically unchanged (Figure 1). After this temperature, a rapid decrease of the crystallinity of the compounds takes place, becoming finally amorphous. Thus, in the 255−585 and 240−720 °C, ranges, for vanadium and iron compounds, respectively, no peaks were observed in the X-ray patterns. These results indicate the existence of a collapse of the crystal structure of these compounds with the loss of the ethylenediammonium cations. The thermodiffractograms of $(C_2H_{10}N_2)_{0.5}[V(HPO_3)_2]$ recordered between 585 and 750 °C show peaks which cannot be identified with phases given in the PDF base data.[6] Above this temperature, the $(VO)_2(P_2O_7)$ phase(*) [$P2_1$ space group with $a = 7.726(1)$, $b = 16.588(1)$, and $c = 9.580(1)$ Å][6c] was detected in the X-ray patterns togeteher with other peaks corresponding to unknown phases. The $Fe_4(P_2O_7)_3$(*), $Fe_3(PO_4)_2$-sarcopside synthetic(+) [$P2_1/c$ space group with $a = 6.014(1)$, $b = 4.773(1)$, $c = 10.405(1)$ Å, and $\beta = 90.94(2)°$] and $Fe_3(PO_4)_2$-graftonite synthetic(|) [$P2_1/c$ space group with $a = 8.886(1)$, $b = 11.182(1)$, $c = 6.148(1)$ Å, and $\beta = 90.35(1)°$][6d]

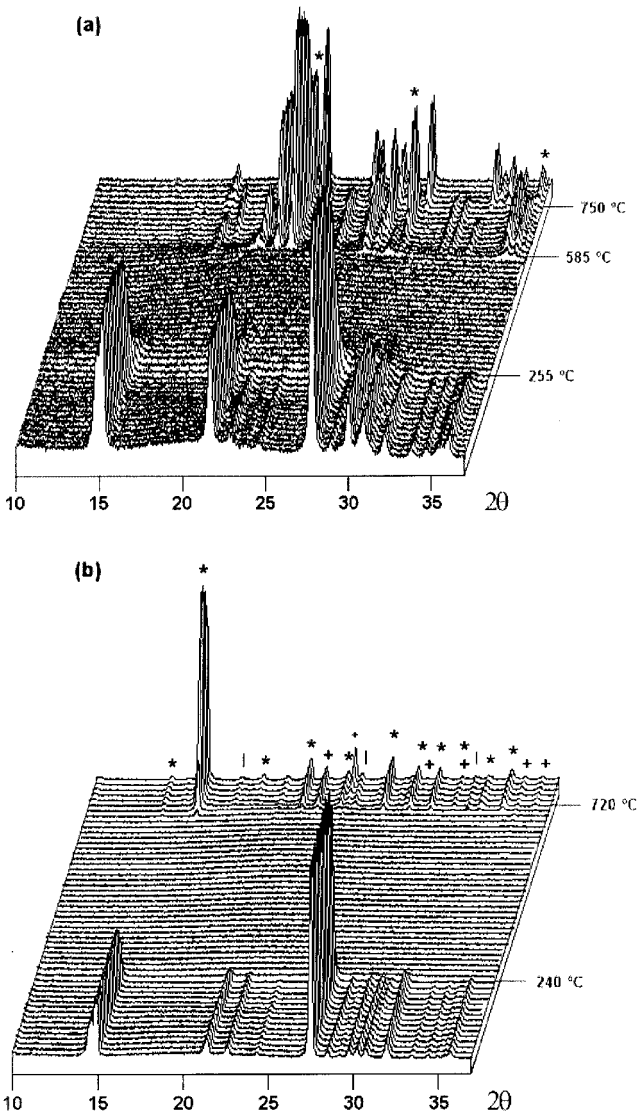


**Figure 1.** Thermodiffractograms of (a) $(C_2H_{10}N_2)_{0.5}[V(HPO_3)_2]$ and (b) $(C_2H_{10}N_2)_{0.5}[Fe(HPO_3)_2]$.

(5) (a) Bonavia, G.; DeBord, J.; Haushalter, R. C.; Rose, D.; Zubieta, J. *Chem. Mater.* **1995**, *7*, 1995. (b) Fernandez, S.; Mesa, J. L.; Pizarro, J. L.; Lezama, L.; Arriortua, M. I.; Olazcuaga, R.; Rojo, T. *Chem. Mater.* **2000**, *12*, 2092. (c) Fernandez, S.; Pizarro, J. L.; Mesa, J. L.; Lezama, L.; Arriortua, M. I.; Olazcuaga, R.; Rojo, T. *Inorg. Chem.* **2001**, *40*, 3476. (d) Fernandez, S.; Pizarro, J. L.; Mesa, J. L.; Lezama, L.; Arriortua, M. I.; Rojo, T. *Int. J. Inorg. Mater.* **2001**, *3*, 331.

(6) Powder Diffraction File−Inorganic and Organic, ICDD, Files No. (a) 84-48 and 71-859, (b) 44-722 and 80-2315, (c) 85-2281, (d) 36-318, 81-695, and 49-1087, Newton Square, PA, 1995.

phases are observed in the X-ray patterns of $(C_2H_{10}N_2)_{0.5}[Fe(HPO_3)_2]$ above 720 °C.

**Collection of Powder X-ray Diffraction Data.** The X-ray powder diffraction data for $(C_2H_{10}N_2)_{0.5}[V(HPO_3)_2]$ were obtained with a STOE STADIP diffractometer using the Debye−Scherrer geometry to minimize preferred orientation effects. The monochromatic Cu K$\alpha_1$ radiaton ($\lambda = 1.5406$ Å), selected with an incident-beam germanium monochromator, was employed. The powder diffraction pattern was scanned over the 5−80° 2$\theta$ angular range, every 0.02° in 2$\theta$, and for 12 s/step. For the $(C_2H_{10}N_2)_{0.5}[Fe(HPO_3)_2]$ compound the X-ray powder diffraction data were collected on a SIEMENS diffractometer with Bragg−Brentano geometry, using Cu K$\alpha$ radiation ($\lambda =$ 1.5418 Å) and equipped with a secondary monochromator to remove the fluorescence radiation from the iron atoms of the compound. The data collection was made in the 5−80° range with a step size of 0.02° in 2$\theta$ and counting time of 12 s/step.

**Ab Initio Structure Determination of $(C_2H_{10}N_2)_{0.5}[V(HPO_3)_2]$.** The angular positions of the first 29 peaks of the X-ray powder diffraction pattern were obtained with the WINPLOTR program.[7] After that, the indexing was performed by using the TREOR 90 program.[8] A monoclinic solution with satisfactory figures of merit [$M_{20} = 19$ and $F_{20} = 30$] and unit cell parameters of $a = 9.35(1)$, $b = 8.82(1)$, $c = 9.26(1)$, $\beta =$ 117(1)°, and $V = 680.1(1)$ Å$^3$ was found. The pattern matching analysis of the diffractogram was carried out by the FULLPROF 98 program,[9] using the unit cell parameters obtained in the indexing and a pseudo-Voigt function for modeling the peak shape. Taking into account the reflections indexed for different monoclinic space groups, the analysis was consistent with the *Pc* and *P*2/*c* space groups. The integrated intensities were extracted with the FULLPROF 98 program[9] and were used as input in the direct methods program SIRPOW 92.[10] A reasonable solution was found in the *Pc* space group, obtaining the atomic coordinates of the V, P, O, C, and N atoms of the compound. This structural model was refined by the Rietveld method, using soft distance constraints for the V−O, P−O, C−N, and C−C bonds. However, high reliability factors and a substantial difference between the observed and calculated powder diffractograms were observed at the end of this process. At this stage, the structural analysis with the PLATON program[11] showed the existence of an inversion center in the structure. So the unit cell parameters and the atomic coordinates transformed according to the *P*2/*c* space group were used in the Rietveld refinement. The refinement converged to satisfactory residual factors and the restraints for the interatomic bond distances, except those for the C−N and C−C bonds, could be eliminated. The final Rietveld refinement was carried out including the atomic coordinates of the hydrogen atoms belonging to the phosphite anions and ethylenediammonium cation, which were previously calculated by using the SHELXL 97 program.[12] The isotropic atomic displacement parameters of the atoms were also included in the refinement. The final reliability factors were $R_B = 4.64$, $R_f = 5.93$, $R_p =$ 15.7, and $R_{wp} =$ 12.0. Crystallographic data and details of the Rietveld refinement are given in Table 1. Figure 2a shows the best agreement obtained between the calculated and observed patterns. Final atomic positional parameters together with the isotropic temperature factors have been deposited as Supporting Information. Selected bond distances and angles are listed in Table 2. All drawings of the structure were made using the ATOMS program.[13]

**Table 1. Summary of Crystallographic Data and Least-Squares Refinement for the $(C_2H_{10}N_2)_{0.5}[M(HPO_3)_2]$ (M = V, Fe) Compounds**

| compound | $CNH_7O_6P_2V$ | $CNH_7O_6P_2Fe$ |
|---|---|---|
| $M$ (g mol$^{-1}$) | 241.9 | 246.8 |
| crystal system | monoclinic | monoclinic |
| space group (No. 13) | *P*2/*c* | *P*2/*c* |
| $a$ (Å) | 9.243(1) | 9.247(1) |
| $b$ (Å) | 8.817(1) | 8.824(1) |
| $c$ (Å) | 9.684(1) | 9.693(1) |
| $\beta$ (deg) | 120.92(2) | 120.72(1) |
| $V$ (Å$^3$) | 677.1(2) | 680.0(1) |
| $Z$ | 4 | 4 |
| $\rho_{calc.}$ (g cm$^{-3}$) | 2.37 | 2.41 |
| $T$ (K) | 298 | 298 |
| radiation Cu K$\alpha$ (Å) | 1.5406 | 1.5418 |
| $\mu$, Cu K$\alpha$ (mm$^{-1}$) | 16.7 | 22.3 |
| 2$\theta$ range (deg) | 5−80 | 5−80 |
| 2$\theta$ step-scan increment (deg) | 0.02 | 0.02 |
| Time step (s/step) | 12 | 12 |
| no. of reflections | 900 | 633 |
| no. of structural parameters | 36 | 39 |
| no. of profile parameters | 12 | 12 |
| $R_p = \Sigma\lvert yi_{obs} - (1/c)yi_{calc}\rvert/\Sigma yi_{obs}$ | 15.7 | 14.1 |
| $R_{wp} = [\Sigma\omega i\lvert yi_{obs} - (1/c)yi_{calc}\rvert^2/\Sigma\omega i[yi_{obs}]^2]^{1/2}$ | 12.0 | 14.5 |
| $R_B = \Sigma\lvert I_{obs} - I_{calc}\rvert/\Sigma I_{obs}$ | 4.64 | 3.59 |
| $R_f = \Sigma\lvert(I_{obs})^{1/2} - (I_{calc})^{1/2}\rvert/\Sigma(I_{obs})^{1/2}$ | 5.93 | 5.03 |
| GOF | 1.71 | 2.24 |

**Rietveld Refinement of $(C_2H_{10}N_2)_{0.5}[Fe(HPO_3)_2]$.** The structure of $(C_2H_{10}N_2)_{0.5}[Fe(HPO_3)_2]$ was refined using the FULLPROF 98 program,[9] modeling the peak shape with a pseudo-Voigt function. The structural parameters of the isostructural vanadium phase were used as a starting model for the Rietveld refinement. Initially, the scale and background variables were refined. After that, subsequent iterations by the zero point of 2$\theta$, the cell constants, and the peak-shape parameters were used in the refinement. The atomic parameters were refined one by one in different stages starting with those corresponding to the elements of the highest scattering factors. From successive refinement cycles the reliability factors dropped to the values $R_B = 3.59$, $R_f = 5.03$, $R_p = 14.1$, and $R_{wp} = 14.5$. The crystal parameters and details of the data collection and structural refinement are shown in Table 1. The observed, calculated, and difference X-ray powder diffraction patterns are shown in Figure 2b. The final positional coordinates and the isotropic temperature factors have been deposited as Supporting Information. Selected bond distances and angles are listed in Table 2. The drawings of the structure were made using the ATOMS program.[13]

**Physical Measurements.** The IR spectra (KBr pellets) were obtained with a Nicolet FT-IR 740 spectrophotometer in the 400−4000-cm$^{-1}$ range. The Raman spectra were recordered in the 200−3000-cm$^{-1}$ range, with a Nicolet 950FT spectrophotometer equipped with a neodymium laser emitting at 1064 nm. Diffuse reflectance spectra were registered at room temperature on a Cary 2415 spectrometer in the 210−2000-nm range. Magnetic measurements on powdered sample were performed in the temperature range 2.0−300 K, using a Quantum Design MPMS-7 SQUID magnetometer. The magnetic field was ≈0.1 T, a value in the range of linear dependence of magnetization vs magnetic field even at 2.0 K.

## Results and Discussion

**Crystal Structure of the $(C_2H_{10}N_2)_{0.5}[M(HPO_3)_2]$ (M = V, Fe) Compounds.** The crystal structure of the $(C_2H_{10}N_2)_{0.5}[M(HPO_3)_2]$ (M= V, Fe) isostructural com-

(7) Roisnel, T.; Rodriguez-Carvajal, J. *WINPLOTR: A New Tool for Powder Diffraction*; Laboratoire Leon Brillouin (CEA-CNRS) Centre d'Etudes de Saclay: Gif sur Yvette Cedex, France, 2000.

(8) Werner, P. E.; Eriksson, L.; Westdahl, M. *TREOR 90: A Semi-exhaustive Trial-and-Error Powder Indexing Program for All Symmetries*; Arrhenius Laboratory, University of Stockholm: Sweden, 1990.

(9) (a) Rodriguez-Carvajal, J. *FULLPROF 98: Program for Rietveld Pattern Matching Analysis of Powder Patterns*, unpublished results, Grenoble, 1998. (b) Rodriguez-Carvajal, J. *Physica B* **1993**, *192*, 55.

(10) Altamontem, A.; Cascarano, G.; Giacovazzo, C.; Guagliardi, A.; Burla, M. C.; Polidori, G.; Camalli, M. *J. Appl. Crystallogr.* **1994**, *27*, 435.

(11) Spek, A. L. *Acta Crystallogr.* **1990**, *A46*, 34.

(12) Sheldrick, G. M. SHELXL 97: *Program for the Refinement of Crystal Structures*; University of Göttingen: Göttingen, Germany, 1997.

(13) Dowty, E. ATOMS: *A Computer Program for Displaying Atomic Structures*; Shape Software: Kingsport, TN, 1993.

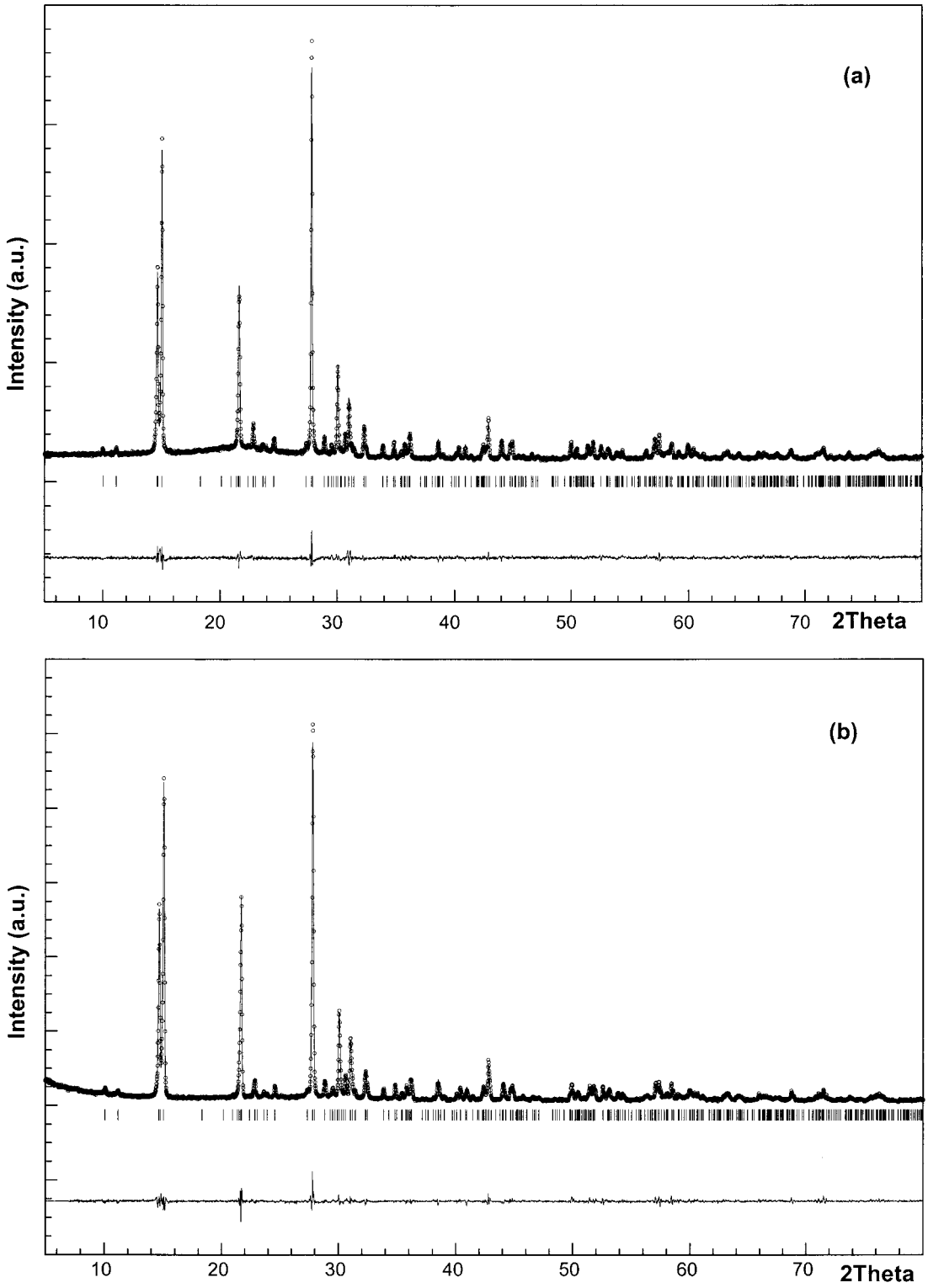


**Figure 2.** Observed, calculated, and difference X-ray powder diffraction patterns of (a) $(C_2H_{10}N_2)_{0.5}[V(HPO_3)_2]$ and (b) $(C_2H_{10}N_2)_{0.5}$-$[Fe(HPO_3)_2]$. The observed data are shown by the dots, the calculated pattern by the solid line, and the difference spectrum in the lower region.

pounds consists of an anionic three-dimensional open framework with $[M(HPO_3)_2]^-$ formula. The charge of this network is compensated by the ethylenediammonium cations, which also establish hydrogen bonds with the inorganic fragment. The structure shows the existence of channels along the *c* axis, where the organic molecules are located (Figure 3).

The vanadium(III) and iron(III) cations adopt an octahedral geometry. Figure 4a shows the connections established between the octahedra and its eight next-nearest neighbors. The $MO_6$ octahedra are linked through the $HP(1)O_3$ and $HP(2)O_3$ phosphite anions to four neighboring octahedra arranged in a diamond-like coordination (see Figure 4b), with an intermetallic distance of ≈5.2 Å. Furthermore, every $MO_6$ octahedron is bonded via the $HP(2)O_3$ phosphite anions to four octahedra with a square-planar geometry (see Figure 4b), in this case the intermetallic distance being ≈6.4 Å.

**Table 2. Selected Bond Distances (Å) and Angles (deg) for $(C_2H_{10}N_2)_{0.5}[M(HPO_3)_2]$ (M = V, Fe) (e.s.d. in Parentheses)[a,b]**

Bond Distances (Å)

| | | | |
|---|---|---|---|
| $V(1)O_6$ Octahedron | | $Fe(1)O_6$ Octahedron | |
| $V(1)-O(1)^{i,ii}$ | 1.90(2) | $Fe(1)-O(1)^{i,ii}$ | 1.94(2) |
| $V(1)-O(3)^{iii,iv}$ | 1.97(1) | $Fe(1)-O(3)^{iii,iv}$ | 2.00(1) |
| $V(1)-O(5)^{v,vi}$ | 1.94(1) | $Fe(1)-O(5)^{v,vi}$ | 1.96(1) |
| $V(2)O_6$ Octahedron | | $Fe(2)O_6$ Octahedron | |
| $V(2)-O(2)^{v,vii}$ | 1.96(1) | $Fe(2)-O(2)^{v,vii}$ | 2.05(1) |
| $V(2)-O(4)^{v,vii}$ | 2.01(1) | $Fe(2)-O(4)^{viii,ix}$ | 2.05(1) |
| $V(2)-O(6)^{i,viii}$ | 1.99(2) | $Fe(2)-O(6)^{i,x}$ | 2.01(2) |
| Metal−Metal | | Metal−Metal | |
| $V(1)-V(2)^{viii}$ | 5.249(5) | $Fe(1)-Fe(2)^{xi}$ | 5.234(4) |
| $V(1)-V(2)^{i}$ | 6.403(7) | $Fe(1)-Fe(2)^{xii}$ | 6.421(6) |
| $V(1)-V(2)^{v}$ | 6.441(7) | $Fe(1)-Fe(2)^{xiii}$ | 6.454(6) |
| $V(1)-V(1)^{ix}$ | 5.200(1) | $Fe(1)-Fe(1)^{xiv}$ | 5.218(3) |
| $HP(1)O_3$ Tetrahedron | | $HP(1)O_3$ Tetrahedron | |
| P(1)−O(4) | 1.52(1) | $P(1)-O(4)^{xv}$ | 1.52(2) |
| P(1)−O(5) | 1.52(1) | P(1)−O(5) | 1.53(1) |
| P(1)−O(6) | 1.46(2) | P(1)−O(6) | 1.44(2) |
| P(1)−H(1) | 1.29(1) | P(1)−H(1) | 1.258(9) |
| $HP(2)O_3$ Tetrahedron | | $HP(2)O_3$ Tetrahedron | |
| P(2)−O(1) | 1.53(2) | P(2)−O(1) | 1.52(2) |
| P(2)−O(2) | 1.58(2) | P(2)−O(2) | 1.48(2) |
| P(2)−O(3) | 1.59(2) | P(2)−O(3) | 1.56(2) |
| P(2)−H(2) | 1.287(9) | P(2)−H(2) | 1.31(1) |
| $(H_3N(CH_2)_2NH_3)^{2+}$ | | $(H_3N(CH_2)_2NH_3)^{2+}$ | |
| N(1)−C(1) | 1.51(2) | N(1)−C(1) | 1.45(3) |
| $C(1)-C(1)^{vii}$ | 1.54(2) | $C(1)-C(1)^{vii}$ | 1.58(3) |
| N(1)−H | 0.89(2) | N(1)−H | 0.89(2) |
| C(1)−H | 0.97(1) | C(1)−H | 0.97(1) |

Bond Angles (deg)

| | | | | | | | |
|---|---|---|---|---|---|---|---|
| $V(1)O_6$ Octahedron | | | | $Fe(1)O_6$ Octahedron | | | |
| $O(1)^{ii}-V(1)-O(3)^{iv}$ | 92.4(7) | $O(5)^{vi}-V(1)-O(3)^{iii}$ | 92.4(5) | $O(5)^{vi}-Fe(1)-O(1)^{ii}$ | 93.0(6) | $O(1)^{ii}-Fe(1)-O(5)^{v}$ | 92.0(6) |
| $O(1)^{ii}-V(1)-O(5)^{v}$ | 91.2(7) | $O(5)^{vi}-V(1)-O(5)^{v}$ | 86.0(5) | $O(5)^{v}-Fe(1)-O(5)^{vi}$ | 87.9(5) | $O(1)^{i}-Fe(1)-O(3)^{iv}$ | 83.9(6) |
| $O(1)^{i}-V(1)-O(5)^{v}$ | 91.4(7) | $O(3)^{iii}-V(1)-O(3)^{iv}$ | 89.4(6) | $O(5)^{v}-Fe(1)-O(1)^{i}$ | 93.0(6) | $O(3)^{iii}-Fe(1)-O(1)^{i}$ | 91.0(6) |
| $O(1)^{iv}-V(1)-O(3)^{iv}$ | 85.0(7) | $O(3)^{iv}-V(1)-O(5)^{v}$ | 92.4(5) | $O(5)^{v}-Fe(1)-O(1)^{iv}$ | 92.9(5) | $O(1)^{i}-Fe(1)-O(5)^{vi}$ | 92.0(6) |
| $O(1)^{i}-V(1)-O(5)^{vi}$ | 91.2(7) | $O(1)^{i}-V(1)-O(1)^{ii}$ | 176.4(7) | $O(3)^{iv}-Fe(1)-O(1)^{ii}$ | 91.0(6) | $O(5)^{v}-Fe(1)-O(3)^{iii}$ | 175.9(8) |
| $O(1)^{i}-V(1)-O(3)^{iii}$ | 92.4(7) | $O(3)^{iv}-V(1)-O(5)^{vi}$ | 175.9(7) | $O(3)^{iii}-Fe(1)-O(3)^{iv}$ | 86.6(6) | $O(1)^{i}-Fe(1)-O(1)^{ii}$ | 172.9(7) |
| $O(1)^{ii}-V(1)-O(3)^{iii}$ | 85.0(7) | $O(5)^{v}-V(1)-O(3)^{iii}$ | 175.9(7) | $O(3)^{iii}-Fe(1)-O(5)^{vi}$ | 92.9(5) | $O(5)^{vi}-Fe(1)-O(3)^{iv}$ | 175.9(8) |
| $O(1)^{ii}-V(1)-O(5)^{vi}$ | 91.4(7) | | | $O(3)^{iii}-Fe(1)-O(1)^{ii}$ | 83.9(6) | | |
| $V(2)O_6$ Octahedron | | | | $Fe(2)O_6$ Octahedron | | | |
| $O(2)^{v}-V(2)-O(2)^{vii}$ | 97.4(6) | $O(2)^{vii}-V(2)-O(6)^{viii}$ | 91.0(7) | $O(2)^{v}-Fe(2)-O(2)^{vii}$ | 98.3(5) | $O(2)^{vii}-Fe(2)-O(2)^{i}$ | 88.4(7) |
| $O(2)^{v}-V(2)-O(6)^{v}$ | 91.0(7) | $O(2)^{vii}-V(2)-O(6)^{i}$ | 87.5(7) | $O(2)^{v}-Fe(2)-O(2)^{ix}$ | 88.4(5) | $O(2)^{vii}-Fe(2)-O(2)^{x}$ | 89.9(7) |
| $O(2)^{v}-V(2)-O(4)^{vii}$ | 88.9(5) | $O(6)^{i}-V(2)-O(4)^{vii}$ | 91.8(6) | $O(2)^{v}-Fe(2)-O(2)^{i}$ | 90.0(7) | $O(2)^{i}-Fe(2)-O(2)^{ix}$ | 89.9(6) |
| $O(2)^{v}-V(2)-O(6)^{viii}$ | 87.5(5) | $O(4)^{vii}-V(2)-O(6)^{viii}$ | 89.9(6) | $O(2)^{v}-Fe(2)-O(2)^{x}$ | 88.4(7) | $O(2)^{ix}-Fe(2)-O(2)^{x}$ | 91.9(6) |
| $O(4)^{v}-V(2)-O(2)^{vii}$ | 88.9(5) | $O(2)^{v}-V(2)-O(4)^{v}$ | 173.6(6) | $O(2)^{viii}-Fe(2)-O(2)^{vii}$ | 88.4(5) | $O(2)^{v}-Fe(2)-O(2)^{viii}$ | 173.1(6) |
| $O(4)^{v}-V(2)-O(6)^{i}$ | 89.9(6) | $O(2)^{vii}-V(2)-O(4)^{vii}$ | 173.6(6) | $O(2)^{viii}-Fe(2)-O(2)^{ix}$ | 84.9(5) | $O(2)^{vii}-Fe(2)-O(2)^{ix}$ | 173.1(6) |
| $O(4)^{v}-V(2)-O(4)^{vii}$ | 84.7(6) | $O(6)^{i}-V(2)-O(6)^{viii}$ | 177.7(7) | $O(2)^{viii}-Fe(2)-O(2)^{i}$ | 91.9(6) | $O(2)^{i}-Fe(2)-O(2)^{x}$ | 177.4(6) |
| $O(4)^{v}-V(2)-O(6)^{viii}$ | 91.8(6) | | | $O(2)^{viii}-Fe(2)-O(2)^{x}$ | 89.9(6) | | |
| $HP(1)O_3$ Tetrahedron | | | | $HP(1)O_3$ Tetrahedron | | | |
| O(4)−P(1)−O(5) | 112(1) | H(1)−P(1)−O(4) | 106.7(8) | $O(4)^{xv}-P(1)-O(5)$ | 108(1) | H(1)−P(1)−O(5) | 102.6(6) |
| O(4)−P(1)−O(6) | 110.0(8) | H(1)−P(1)−O(5) | 105.2(6) | $O(4)^{xv}-P(1)-O(6)$ | 115.7(8) | H(1)−P(1)−O(6) | 97.3(8) |
| O(5)−P(1)−O(6) | 118(1) | H(1)−P(1)−O(6) | 103.6(9) | O(5)−P(1)−O(6) | 118.8(9) | $H(1)-P(1)-O(4)^{xv}$ | 113.5(8) |
| $HP(2)O_3$ Tetrahedron | | | | $HP(2)O_3$ Tetrahedron | | | |
| O(1)−P(2)−O(2) | 116.3(8) | H(2)−P(2)−O(1) | 98(1) | O(1)−P(2)−O(2) | 114.0(8) | H(2)−P(2)−O(1) | 98.8(9) |
| O(1)−P(2)−O(3) | 115.7(9) | H(2)−P(2)−O(2) | 121.4(8) | O(1)−P(2)−O(3) | 115.0(9) | H(2)−P(2)−O(2) | 111.0(7) |
| O(2)−P(2)−O(3) | 103(1) | H(2)−P(2)−O(3) | 102.1(6) | O(2)−P(2)−O(3) | 102(1) | H(2)−P(2)−O(3) | 116.1(6) |
| $(H_3N(CH_2)_2NH_3)^{2+}$ | | | | $(H_3N(CH_2)_2NH_3)^{2+}$ | | | |
| $N(1)-C(1)-C(1)^{vii}$ | 111(1) | | | $N(1)-C(1)-C(1)^{vii}$ | 112(1) | | |

[a] Symmetry codes for the vanadium phase: i = $-x+1, -y, -z$. ii = $x-1, -y, z-1/2$. iii = $x-1, y-1, z-1$. iv = $-x+1, y-1, -z+1/2$. v = $x, y, z$. vi = $-x, y, -z-1/2$. vii = $-x+1, y, -z+1/2$. viii = $x, -y, z+1/2$. ix = $-x, -y-1, -z$. [b] Symmetry codes for the iron phase: i = $-x+1, -y+1, -z+1$. ii = $x-1, -y+1, z+1/2$. iii = $x-1, y, z$. iv = $-x+1, y, -z+3/2$. v = $x, y, z$. vi = $-x, y, -z+3/2$. vii = $-x+1, y, -z+1/2$. viii = $x, y-1, z$. ix = $-x+1, y-1, -z+1/2$. x = $x, -y+1, z-1/2$. xi = $-x+1, -y+1, -z+1$. xii = $x, y, z+1$. xiii = $x, y+1, z+1$. xiv = $-x, -y+1, -z+2$. xv = $x, y, z+1$.

In the vanadium(III) and iron(III) compounds the metallic cations of the $M(1)O_6$ octahedra are bonded to the O(1), O(3)-oxygen atoms belonging to the $HP(2)O_3$ anion and to the O(5)-oxygen from the $HP(1)O_3$ one. The mean M(1)−O bond distances are 1.94(3) and 1.97(3) Å for the vanadium and iron compounds, respectively. In the $M(2)O_6$ octahedra the links of the metallic cations to the $HP(2)O_3$ and $HP(1)O_3$ phosphite groups are established through the O(2) and O(4), O(6) atoms, respectively. The mean M(2)−O bond distances are 1.99(3) Å for the vanadium phase and 2.04(2) Å for the iron compound. In the vanadium(III) compound, the *cis*- and *trans*-O−M−O angles belonging to the $MO_6$ octahedra range from 84.7(6) to 97.4(6)° and from 173.6(6) to 177.7-

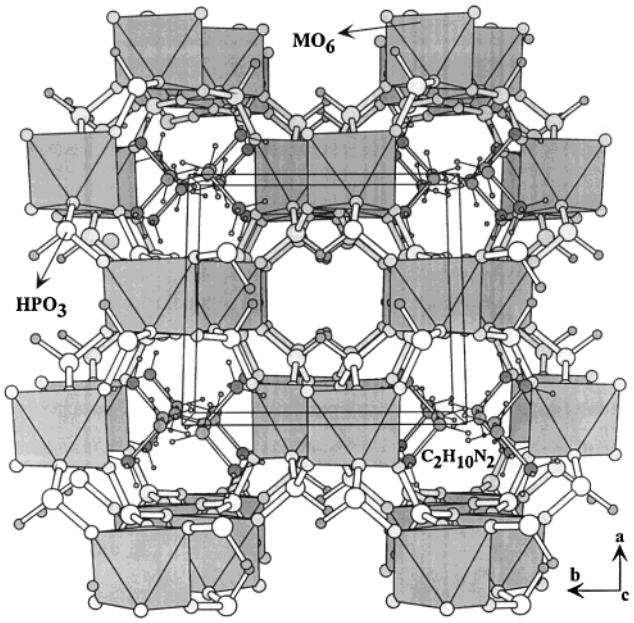


**Figure 3.** Polyhedral view along the [001] direction of the $(C_2H_{10}N_2)_{0.5}[M(HPO_3)_2]$ (M = V, Fe) compounds showing the channels with the ethylenediammonium cations.

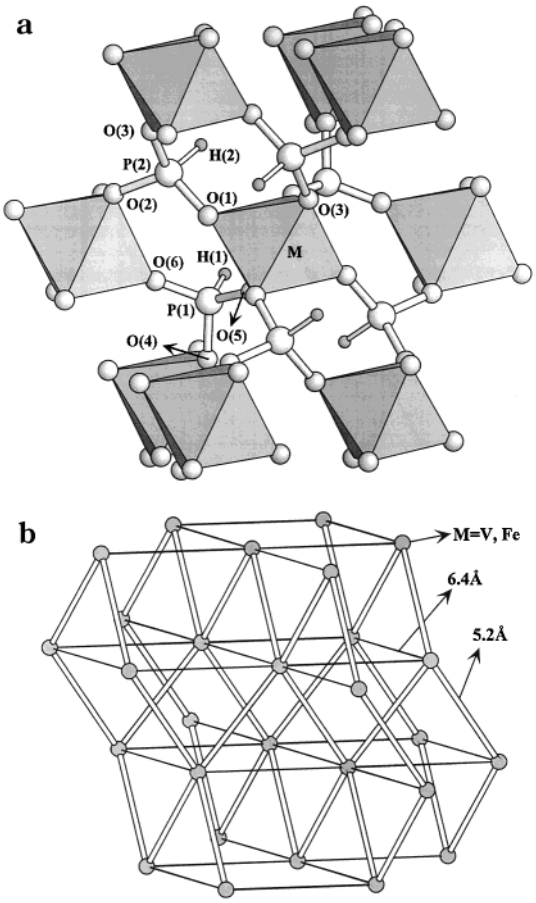


**Figure 4.** (a) View of the connections of an octahedron to its eight next-nearest neighbors with detalled labeling of the atoms. (b) Tetrahedral and square-planar arrangements of the metallic cations.

(7)°, respectively. For the iron(III) compound the *cis*- and *trans*-O−M−O angles are in the 84.9(5)−98.3(5)° and 173.1(6)−177.4(6)° ranges, respectively. The distortion of the $MO_6$ polyhedra from an octahedron to a trigonal bipyramid, calculated by quantification of the Muetterties and Guggenberger description,[14] is smaller than 5%, which indicates a topology near an octahedron.

The P−O and P−H bonds of the $HPO_3$ tetrahedra for the vanadium(III) phase exhibit mean values of 1.53(5) and 1.29(1) Å, respectively. In the case of the iron(III) compound the values are 1.51(4) and 1.30(2) Å. The O−P−O and H−P−O angles show values usually found in tetrahedral coordination. In both compounds the ethylenediammonium cations form hydrogen bonds with the oxygen atoms from the phosphite anions.

**Infrared and Raman Spectroscopies of the $(C_2H_{10}N_2)_{0.5}$ $[M(HPO_3)_2]$ (M = V, Fe) Compounds.** The infrared and Raman spectra of the $(C_2H_{10}N_2)_{0.5}[V(HPO_3)_2]$ and $(C_2H_{10}N_2)_{0.5}[Fe(HPO_3)_2]$ phases exhibit in all cases the bands corresponding to the vibrations of the ethylenediammonium cations and the $(HPO_3)^{2-}$ phosphite anions. Selected bands obtained from both the IR and Raman spectra are given in Table 3. The results are similar to those found in the literature for other ethylenediammonium phases.[15]

**UV−Vis Spectroscopy of the $(C_2H_{10}N_2)_{0.5}[M(HPO_3)_2]$ (M = V, Fe) Compounds.** The reflectance diffuse spectrum of $(C_2H_{10}N_2)_{0.5}[V(HPO_3)_2]$ shows the spin-allowed transitions from the fundamental state $^3T_{1g}(^3F)$ to the excited levels $^3T_{2g}(^3F)$, $^3T_{1g}(^3P)$, and $^3A_{2g}(^3F)$ at the frequencies 14160, 21420, and 29460 $cm^{-1}$, respectively. Furthermore, the spin-forbidden transition $^3T_{1g}(^3F) \rightarrow {}^1E_g(^1D)$, $^1T_{2g}(^1D)$ was observed as a shoulder on the first band at 10175 $cm^{-1}$. The values obtained of the Dq and Racah parameters were, Dq = 1530 $cm^{-1}$, B = 560 $cm^{-1}$, and C = 3220 $cm^{-1}$. These results are in good agreement with those observed for the V(III) ions in an octahedral environment.[16] The value obtained for the B parameter is ≈65% of that corresponding to the $V^{3+}$ ion (861 $cm^{-1}$), which indicates the existence of a significant covalence character in the V−O chemical bonds.

In the diffuse reflectance spectrum of $(C_2H_{10}N_2)_{0.5}[Fe(HPO_3)_2]$ bands at 13930, 20265, 24010, and 26710 $cm^{-1}$ are observed. The intensity of these bands is weak, as expected, for the spin-forbidden transitions between the ground state $^6A_{1g}(^6S)$ and the excited levels $^4T_{1g}(^4G)$, $^4T_{2g}(^4G)$, $^4A_{1g}(^4G)$,$^4E_g(^4G)$, and $^4T_{2g}(^4D)$ of a $d^5$ high-spin cation in regular octahedral symmetry.[16c] The values calculated for Dq = 1120 $cm^{-1}$, B = 900 $cm^{-1}$, and C = 3000 $cm^{-1}$ are in the range habitually found for the iron(III) cation.[16c] The reduction of the B-parameter value with respect to that of the free ion (1150 $cm^{-1}$) is ≈80%, suggesting a significant covalence in the Fe−O bonds.

**Magnetic Properties of the $(C_2H_{10}N_2)_{0.5}[M(HPO_3)_2]$ (M = V, Fe) Compounds.** Magnetic measurements of the $(C_2H_{10}N_2)_{0.5}[M(HPO_3)_2]$ (M = V, Fe) compounds were performed on powdered samples from room temperature to 2.0 K. Plots of $\chi_m$ and $\chi_m T$ curves for the vanadium

(14) Muetterties, E. L.; Guggenberger, L. J. *J. Am. Chem. Soc.* **1974**, *96*, 1748.

(15) (a) Gharbi, A.; Jouini, A.; Averbuch-Pouchot, M. T.; Durif, A. *J. Solid State Chem.* **1994**, *111*, 330. (b) Dolphin, D.; Wick, A. E. *Tabulation of Infrared Spectral Data*; John Wiley & Sons: New York, 1977. (c) Tsuboi, M. *J. Am. Chem. Soc.* **1957**, *79*, 1351. (d) Nakamoto, K. *Infrared and Raman Spectra of Inorganic and Coordination Compounds*; John Wiley & Sons: New York, 1997.

(16) (a) Mason, W. R.; Gray, H. B. *J. Am. Chem. Soc.* **1968**, *90*, 5721. (b) Sutton, J. E.; Krentzien, H.; Taube, H. *Inorg. Chem.* **1980**, *19*, 2425. (c) Lever, A. B. P. *Inorganic Electronic Spectroscopy*: Elsevier Science Publishers B.V.: Amsterdam, The Netherlands, 1984.

**Table 3. Selected Bands (Values in cm$^{-1}$) from the IR and Raman Spectra for the $(C_2H_{10}N_2)_{0.5}[M(HPO_3)_2]$ (M = V, Fe) Compounds[a]**

| | M = V | | M = Fe | |
|---|---|---|---|---|
| assignment | IR | Raman | IR | Raman |
| $\nu(-NH_3)^+$ | 3040 (m) | 3040 (m) | 3040 (m) | 3040 (m) |
| $\nu(-CH_2-)$ | 3210−2930 (m) | 2995 (m) | 3205−2920 (m) | 3040−2995 (m) |
| $\nu$(HP) | 2385 (m) | 2395, 2375 (s) | 2385(m) | 2390, 2380 (s) |
| $\delta(-NH_3)^+$ | 1595 (m) | 1590 (m) | 1590 (m) | 1605 (m) |
| $\delta(-CH_2-)$ | 1520−1460 (m) | 1470 (w) | 1520−1460 (m) | 1525−1460 (m) |
| $\nu_{as}(PO_3)$ | 1110 (m) | 1105 (m) | 1115 (m) | 1105 (m) |
| $\delta$(HP) | 1070 (s) | 1060, 1030 (s) | 1065 (s) | 1085, 1025 (s) |
| $\nu_s(PO_3)$ | 1005 (w,sh) | 1000 (m) | 1000 (w,sh) | 1000 (m) |
| $\delta_s(PO_3)$ | 605 (m) | 610 (w) | 600 (m) | 610 (w) |
| $\delta_{as}(PO_3)$ | 510 (m) | 540 (m) | 490 (m) | 510 (m) |

[a] $\nu$ = stretching. $\delta$ = deformation. s = symmetric. as = asymmetric. w = weak. m = medium. s = strong. sh = shoulder.

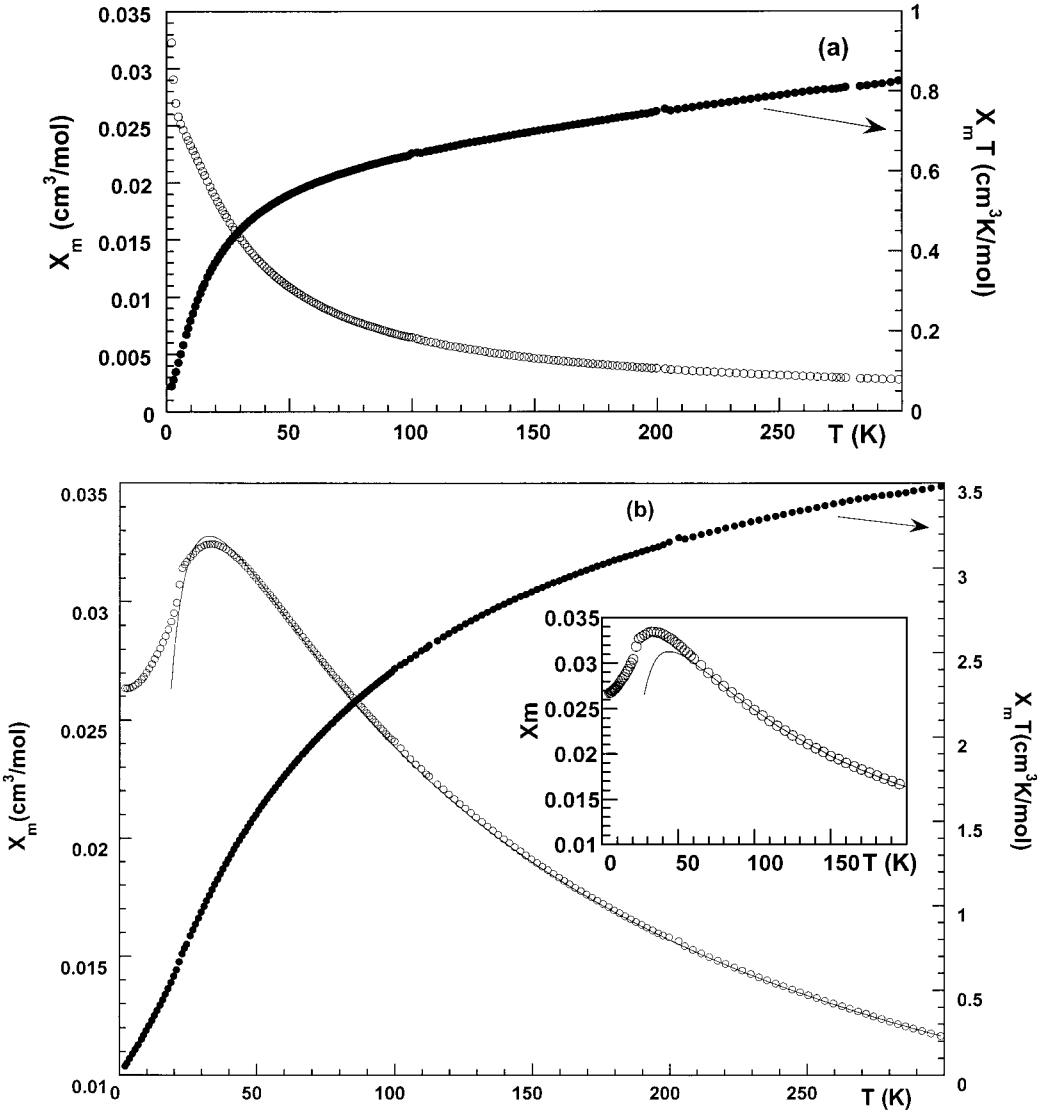


**Figure 5.** Thermal evolution of $\chi_m$ and $\chi_m T$ curves of the (a) vanadium and (b) iron compounds. The solid lines in (b) show the fit of the $\chi_m$ data to a model for an antiferromagnetic three-dimensional diamond-like network.

compound are shown in Figure 5a. The molar magnetic susceptibility of this phase increases with decreasing temperature in the temperature range studied. The thermal evolution of $\chi_m$ follows the Curie−Weiss law at temperatures higher than 10 K, with Cm = 0.90 cm$^3$·L/mol and $\theta = -34.7$ K. The $\chi_m T$ product decreases from 0.83 cm$^3$·K/mol at 300 K to 0.06 cm$^3$·K/mol at 2.0 K. These results indicate the existence of antiferromagnetic interactions in this compound.

The thermal evolution of the $\chi_m$ and $\chi_m$T curves for the iron compound is given in Figure 5b. The $\chi_m$ vs $T$ curve follows the Curie−Weiss law for temperatures higher than 70 K, with Cm = 4.63 cm$^3$·K/mol and $\theta = -88.4$ K. The molar magnetic susceptibility increases from room temperature with decreasing temperature and reaches a maximum at ≈33 K, indicating that a long magnetic ordering, probably three-dimensional in nature, is established at this temperature. Below 33 K

the magnetic susceptibility continuously decreases up to 2.0 K. This result together with the continuous decrease in the $\chi_m T$ vs $T$ curve, from 3.55 $cm^3 \cdot K/mol$ at room temperature to 0.07 $cm^3 \cdot K/mol$ at 2.0 K, is indicative of antiferromagnetic exchange couplings in this compound, which are stronger than those observed in the vanadium phase.

These results suggest, at first glance, that both compounds could be interpreted as three-dimensional magnetic systems, which is supported by the structural features. However, the value of the magnetic susceptibility in the maximum of the $\chi_m$ vs $T$ curve of $(C_2H_{10}N_2)_{0.5}[Fe(HPO_3)_2]$ does not acquire the value of $^2/_3$ of the magnetic susceptibility extrapoled at 0 K, as expected for a three-dimensional magnetic system.[17] From the magnetic point of view a more realistic approximation to the problem would be to consider the three-dimensional framework of these compounds as formed by two sublattices with tetrahedral and square-planar geometries (see Figure 4b). In this way, the magnetic data of $(C_2H_{10}N_2)_{0.5}[Fe(HPO_3)_2]$ were fitted to a model for an antiferromagnetic-like diamond network of spin $S = {}^5/_2$, by using the Rushbrooke and Wood equation (eq 1),[18]

$$\chi_m = (35N\beta^2g^2/12kT)(1 - 23.3333x + 147.7777x^2 - 405.4815x^3 + 1621.1265x^4 + 14200.9693x^5 - 1037844.156x^6)^{-1} \quad (1)$$

where $x = |J|/kT$, $k$ is the Boltzmann constant, $N$ is Avogadro's number, and $\beta$ is the Bohr magneton. The results are given in Figure 5b. As can be seen in the inset of this figure, it was not possible to fit simultaneously the temperature of the maximum of the magnetic susceptibility curve and its value at this temperature. Considering the approximation of the molecular field,[17] a reasonable good fit to the magnetic data was obtained (see Figure 5b). The exchange parameters are $J = -2.1$ K, $J' = -1.3$ K, with $g = 2.01$ and $z = 4$. However, the very high value obtained for the $J'$ parameter indicates that these results should be considered with caution and show that a significant contribution of the square-planar network to the magnetic exchange should be considered. Attempts to fit the magnetic data of $(C_2H_{10}N_2)_{0.5}[Fe(HPO_3)_2]$ to a model for antiferromagnetic square-planar network by using the Rushbrooke and Wood expression[18] were unsuccessful. In the case of $(C_2H_{10}N_2)_{0.5}[V(HPO_3)_2]$ it was not possible to perform any reasonable fit of the magnetic data owing to the absence of a maximum in the thermal evolution of the magnetic susceptibility.

These results are in accordance with the structural features of these compounds, in which it can be observed that the metallic cations of the tetrahedral network are linked by two phosphite anions and separated by ≈5.2 Å. Conversely, in the square-planar network the connection is only through a phosphite group, the intermetallic distance being ≈6.4 Å. Taking into account these structural data, it seems reasonable to consider that the superexchange magnetic interactions are principally propagated via tetrahedral geometry and complemented with those corresponding to the square-planar arrangement. Furthermore, this kind of intermetallic connection through phosphite anions should favor the antiferromagnetic exchange couplings,[19] as observed in these compounds.

## Concluding Remarks

Two new inorganic−organic hybrid materials based on vanadium(III) and iron(III) cations and the $(HPO_3)^{2-}$ phosphite oxoanion have been synthesized by hydrothermal reactions as polycrystalline powdered samples. Ab initio methods have been used to solve the crystal structure of these compounds from powdered diffraction data. The compounds exhibit a three-dimensional structure with channels where the templating ethylenediamine molecules are located. The metallic cations form two sublattices with tetrahedral diamond-like and square-planar geometries. The ethylenediammonium cations of the channels were removed with loss of crystallinity and collapse of the inorganic network. The spectroscopic data in the visible region confirm the presence of the metallic cations in slightly distorted octahedral geometry. The magnetic measurements of both compounds indicate the presence of antiferromagnetic interactions, being smaller in the vanadium compound. The $J$-exchange parameter of the iron compound, approximately −2 K, was estimated by fitting the magnetic data to a diamond-like network. However, it is worth noting the presence of an appreciable contribution from the square-planar sublattice in the magnetic interactions of this compound.

**Acknowledgment.** This work was financially supported by the Ministerio de Educación y Ciencia (PB97-0640; BQU2001-0678) and Universidad del País Vasco/EHU (169.310-EB149/98; 9/UPV00169.310-13494/2001), which we gratefully acknowledge. S. Fernandez thanks the Gobierno Vasco/Eusko Jaurlaritza for a doctoral fellowship.

**Supporting Information Available:** Listing of details of the X-ray powder structural resolution (PDF). This material is available free of charge via the Internet at http://pubs.acs.org.

CM0112845

(17) Carlin, R. L. *Magnetochemistry*; Springer-Verlag: Berlin, 1986.
(18) Rushbrooke, G. S.; Wood, P. J. *Mol. Phys.* **1958**, *1*, 257.
(19) Lezama, L.; Shu, K. S.; Villeneuve, G.; Rojo, T. *Solid State Commun.* **1990**, *76*, 449.